Mn 3d majority spin states in c (2 × 2) Mn/fcc-X(001) systems (X = Fe, Co, Ni, Cu)

Mn 3d majority spin states in c(2 × 2) Mn/fcc-X(001) systems (X = Fe, Co, Ni, Cu)

F Schiller[1,4]**, S V Halilov**[2,3] **and C Laubschat**[1]

[1] Institut für Festkörperphysik, TU Dresden, 01062 Dresden, Germany
[2] Center for Computational Materials Science, Naval Research Laboratory, Washington, DC 20375, USA
[3] DMSE, University of Pennsylvania, Philadelphia, PA 19104, USA

Abstract
Results of an angle-resolved photoemission study of the 0.5 monolayer c(2 × 2) manganese superstructure on fcc-(001) surfaces of Fe, Co, Ni, and Cu are presented. In order to stabilize an fcc structure of Fe and Co, thin films of these ferromagnetic metals were grown pseudomorphically on Cu(001). For comparison, linear muffin-tin orbital band structure calculations were carried out to identify the contributions of the atoms of the surface compound to the density of states. For Mn on Cu(001) and Ni(001) the position of the manganese 3d majority spin band at the $\bar{\Gamma}$-point of the second surface Brillouin zone is found at 3.0 eV, while for Mn on Fe/Cu(001), Co/Cu(001), and Ni/Cu(001) the band position is shifted to 3.5 eV binding energy. The identical binding energy position on all ferromagnetic thin films substrates is attributed to the negligible hybridization of the Mn 3d majority spin band while on Cu(001) Mn bands can hybridize with copper derived states, resulting in a slightly different energy position. Furthermore, a decrease of the lattice constant results in a decrease in binding energy consistent with the picture of local magnetic Mn 3d moments.

(Some figures in this article are in colour only in the electronic version)

1. Introduction

The electronic and magnetic structure of ultrathin films, particularly that of two-dimensional surface structures, may strongly deviate from that in three dimensions. The violation of the symmetry at the surface may introduce new electronic (surface) states and change the magnetic properties. Manganese is of special interest since in the Mn atom half of the 3d shell is filled, yielding the highest magnetic atomic moment of 5 μ_B among the 3d atoms. Mn-based

---

[4] Present address: Donostia International Physics Center, Manuel Lardizabal 4, E-20018 Donostia/San Sebastián, Spain.

compounds are therefore expected to differ in their magnetic properties from their constituents. Surface compounds of manganese should further increase such effects.

The aim of this contribution is the analysis of the Mn 3d majority spin band position by means of photoemission when 0.5 monolayer (ML) of manganese is deposited onto the fcc(001) surfaces of Fe, Co, Ni, and Cu. Already the pure fcc(001) surfaces of Fe, Co, and Ni represent different magnetic ground states and hence different magnetic coupling of the Mn atoms to the magnetic hosts can take place. Furthermore, using magnetic (Fe, Co, Ni) or non-magnetic (Cu) substrates will affect electronic and magnetic properties of the submonolayer Mn film although the structure of the surface layer is identical. Here we will focus only on the position of the Mn majority spin band at the centre of the surface Brillouin zone since the minority spin band was found to be unoccupied.

Half a monolayer of manganese deposited onto Cu(001) and Ni(001) forms ordered c(2 × 2) MnCu and c(2 × 2) MnNi surface compounds, respectively, where the face centred atoms of the substrate are replaced by Mn atoms [1] shifted by 0.3 Å out of the surface plane [2–7]. The driving force for this surface structure is the magnetism of the system that stabilizes the surface corrugation [4]. A similar c(2 × 2) superstructure in the low energy electron diffraction (LEED) pattern has also be observed for Mn deposited on the (001)-face of pseudomorphic grown fcc-Co/Cu(001) films [8] and the same structure as for Mn/Cu(001) and Mn/Ni(001) was concluded. The Mn atoms couple ferromagnetically to Ni and Co in the c(2 × 2) MnNi and MnCo surface compounds, respectively, as proved by measurements of circular dichroism [9, 10] and magneto-optical Kerr effect [11]. For c(2 × 2) MnCu/Cu(001) manganese atoms are in a high spin ground state [12, 9] and evidence for a long-range order below 50 K was found [13]. Theoretical investigations of the c(2 × 2) MnCu/Cu(001) surface compound suggest a ferromagnetic ground state and local Mn magnetic moments between 3.75 and 4.09 μ_B [14–16], values close to the Mn free atom value of 5 μ_B. In c(2 × 2) MnNi the magnetic moment of the Mn atoms (3.5 μ_B) is slightly lower than in c(2 × 2) MnCu [14, 15]. Experimentally, the Mn 3d band was found to be split into majority spin components at 3.7 and 3.0 eV below the Fermi energy (E_F) and minority spin components at 1.85 and 2.05 eV above E_F for Mn/Cu(001) and Mn/Ni(001), respectively [15]. Theoretical studies predict spin splitting between 2.7 eV [15] and 4.4 eV [16], values that are considerably smaller than the experimental results. The discrepancy was ascribed to final state effects occurring in the photoemission process [15]. Angle resolved photoemission (PE) experiments on c(2 × 2) MnCu found part of the Mn 3d majority spin band occupied at the $\bar{\Gamma}$ point of the second surface Brillouin zone (SBZ) at 3.0 eV binding energy (BE) [17]. Additionally, at special points of the surface Brillouin zone occupied minority spin states were observed [18, 19]. While the Mn/Cu(001) surface is very well studied [15, 17, 19–22] by photoemission, no information is available about the c(2 × 2) surface compounds of MnNi, MnCo, and MnFe apart from the above mentioned MnNi results.

In the present work fcc substrate surfaces of Fe, Co, Ni, and Cu will be used, the former ones grown epitaxially on Cu(001). Therefore, in the following the growth of these materials on the Cu(001) substrate will be briefly described. It will be shown that the films reveal fcc structures with (001) orientation of the surface plane and no trace of Cu segregation at the surface. The last point is important since we will investigate surface compounds of the ferromagnetic and the Mn atoms that could be falsified by possible MnCu surface alloying if Cu atoms existed at the surface.

The growth mode of Co/Cu(001) at very low coverage is still not clear and both layer-by-layer [23] and bilayer growth [24] have been reported. Recent investigations found a bimodal growth mode where a few Co atoms at Cu sites act as nucleation points for the formation of a Co layers [25] and are probably responsible for the different experimental findings. At

larger coverage growth occurs in a layer-by-layer mode reproducing the Cu(001) fcc substrate structure but with a smaller interlayer distance perpendicular to the surface caused by the smaller atomic volume of the Co atoms. This results in a tetragonal distorted face centred structure that maintains the unit cell volume of hcp Co. For low coverage (up to 4 ML) a small amount of copper (<10%) remains at the surface upon room temperature deposition [24]. Investigations of the three-layer system Mn/Co/Cu(001) differ in their structural results: while O'Brien and Tonner observed a p(1 × 1) superstructure [26], Choi *et al* report a c(2 × 2) LEED pattern [8]. In the latter case, the c(2 × 2) superstructure is assigned to the formation of a two-dimensional MnCo surface compound as in MnCu and MnNi.

The initial growth mode of Fe/Cu(001) has also been discussed controversially. Layer-by-layer and bilayer as well as island growth and intermixing were reported (see [27] and references therein). At 2 ML coverage a (4 × 1) reconstruction is obtained, that transforms into a (5 × 1) structure at 4 ML [27]. Above 5 ML a (2 × 1) superstructure replaces the latter and a collapse of Fe islands takes place followed by a layer-by-layer growth mode [28]. The individual superstructures are related to different magnetic properties. The magnetization vector switches from in plane to a perpendicular out-of-plane direction when exceeding 5 ML. Above 11 ML iron grows in a bcc lattice on Cu(001) [27]. No investigation of the Mn/Fe/Cu(001) interface has been elaborated so far.

Ni films on Cu(001) form pseudomorphic layers which are strained up to a critical thickness of about 7 ML [29, 30]. Above a coverage of 7 ML and up to at least 10 ML misfit dislocations are formed that are energetically preferred as compared to the strained layer [29]. The magnetization vector changes dependent on temperature from in-plane magnetization at low coverage to perpendicular to the surface above 7 ML (200 K) [31], while Ni single crystals reveal in-plane magnetization at the (001) surface. This spin reorientation transition was addressed to the tetragonal distortion of the growing Ni film [32]. Surprisingly, there exist very few publications about the electronic structure of thin Ni films and the reported results are controversial [33, 34]. While Mankey *et al* [33] obtain already after 1 ML Ni/Cu a Ni bulk-like electronic structure, Pampuch and co-workers [34] found this limit at higher coverage (3 ML). Scanning tunnelling microscopy investigations of the film reveal a closed surface and a layer-by-layer mode of growth [30]. Spišák and Hafner calculated the effect of possible Cu segregation leading to a Cu layer on top of the Ni film and found its formation energetically preferred even for 5 ML Ni/Cu(001) [35]. For 1 ML Ni/Cu(001) the presence of a Cu layer on top of the Ni film was also observed by Kim *et al* [36]. PE studies, however, taken at a photon energy of 43 eV, that is very surface sensitive, found the intensity of copper derived emissions to be negligible for a coverage of 6 ML Ni/Cu(001) [34].

First we will describe our experimental and theoretical details (sections 2 and 3). The Mn/Fe/Cu(001) system is studied here for the first time, therefore section 4 will deal with the growth of Mn onto Fe/Cu(001) thin films with two different thicknesses. Next we describe the method that we use to determine the position of the Mn majority spin band probed in the Mn/Cu(001) system (section 5.1). Results for Mn deposition on the thin film surfaces of Fe, Co, and Ni obtained by the same method will be discussed in section 5.2. Conclusions are drawn in the last section.

2. Experiment

PE experiments were carried out in an ultrahigh vacuum apparatus equipped with an angle resolved hemispherical Scienta-200 electron analyser and a six-axis sample manipulator as described elsewhere [22].

The single-crystalline Cu(001) and Ni(001) substrates were cleaned by cycles of Ar$^+$ bombardment at 1000 and 500 V followed by annealing at 500 °C for about 5 min to rearrange the surface structure. Structural order was checked by LEED that exhibited sharp p(1 × 1) spots after cleaning. The presence of contamination was checked by monitoring carbon and oxygen related core level and valence band signals by means of photoemission and was found to be negligible. Pure manganese metal (99.98%) was evaporated from a tantalum crucible. In order to decrease surface contaminations, the manganese evaporator was carefully degassed, guaranteeing a pressure below 1×10^{-7} Pa during Mn deposition. The Mn evaporation rate was tuned to about 1 monolayer (ML) per minute. Coverage of 0.5 ML Mn was calibrated by optimizing the c(2 × 2) LEED pattern in the Mn/Cu(001) system as described by Flores *et al* [1]. During the PE experiment the base pressure was 6×10^{-9} Pa. As suggested in [15] Mn deposition onto the Ni(001) single crystal was carried out at 300 °C substrate temperature that increased considerably the quality of the LEED pattern as compared to room temperature preparation.

Fe(001), Co(001), and Ni(001) thin film surfaces were prepared at room temperature by thermal deposition of 2–7 ML of the respective material on Cu(001). The metals were evaporated from pure metallic rods (99.99%) by means of electron impact.

3. Theory

Linear muffin-tin orbital band structure calculations [37] in the atomic sphere approximation (LMTO-ASA) were performed for a c(2 × 2)MnCu six-layer Cu super-cell with empty monolayers on one ('vacuum') side of the MnCu compound layer for better simulation of the near-surface region. Empty spheres in that region were added in order to account for effects of non-spherical spatial distribution of the charge density, although with limited accuracy. Consistent with earlier theoretical results a ferromagnetic ground state was assumed for the c(2 × 2) MnCu surface compound [4, 16]. Within the local spin density approximation (LSDA) to density functional theory (DFT), the obtained spin moments of the Mn and Cu atoms in the MnCu surface compound correspond to 3.83 and 0.095 μ_B, respectively, assuming ferromagnetic (FM) ordering. Buckling of the Mn atoms within the compound layer of 0.3 Å was taken into account. Since differences to the unbuckled MnCu layer were found to be negligible, calculations for the other c(2 × 2) MnX/X super-cell structures (X = Fe, Co, Ni) were modelled without buckling. Experimentally, Fe, Co, and Ni grow on Cu(001) with tetragonal distortion perpendicular to the surface. The tetragonal distortion (5% deviation of the lattice constant) represents an interlayer effect and affects the LDOS much more weakly than the intralayer interaction (hybridization of Mn and X atoms). It did not lead to changes in the Mn/Ni system and was, therefore, neglected in the calculations. Furthermore, empty layers were not considered in the case of Mn/Fe and Mn/Ni systems since the high density of states at the Fermi level induced numerical instabilities when empty layers were added. As will be shown below, in the cases of the ferromagnets, hybridization effects with Mn will dominate the local DOS. Inclusion of an empty layer would cause minor changes, e.g., narrowing of the peaks in the DOS. Our analysis of the magnetic ground state revealed that the ferromagnetic solution does not correspond to the lowest total energy in all cases. For c(2 × 2) MnCo/Co(001) as well as for c(2 × 2) MnFe/Fe(001) an ferrimagnetic (ferriM) solution was energetically preferred, i.e., Mn moments couple antiparallel to Co and Fe atoms in the surface compound. This finding is in agreement with previous theoretical predictions for MnCo [38] and MnFe [39]. However, the calculated total energies of ferromagnetic and ferrimagnetic configurations differ only very slightly and may be falsified by the neglect of the empty spheres in the Mn/Fe case. The calculated layered densities of states (LDOSs) for lowest total energy are shown in figure 1;
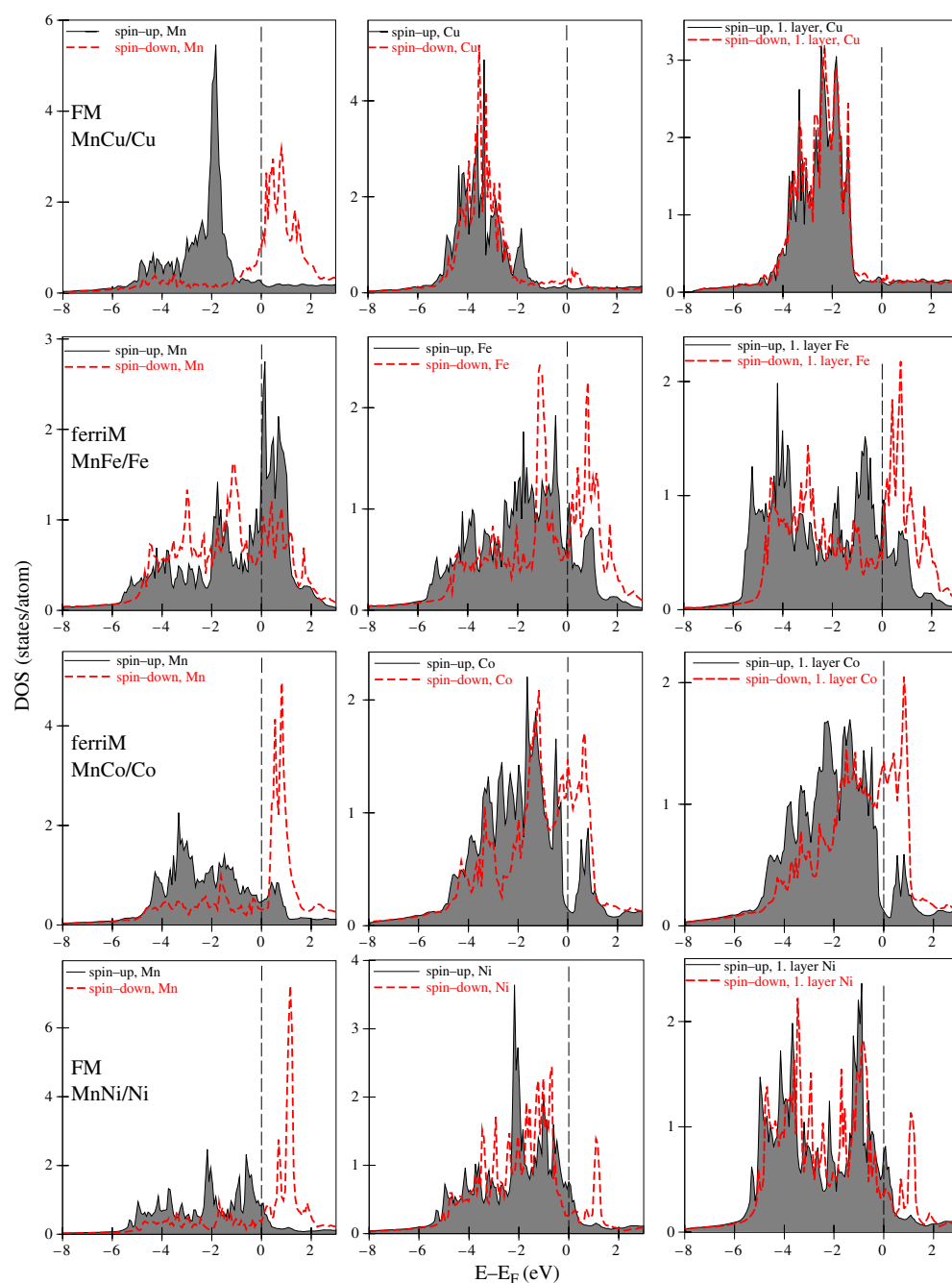
Figure 1. Local density of states at the Mn (left) and X (middle) atom of the c(2 × 2) MnX/X(001) surface compounds (X = Cu, Fe, Co, and Ni) and of the X atom in the first layer (right), respectively. Spin-up and down are used for the spin projection parallel and anti-parallel to the local magnetization.

the corresponding magnetic moments are presented in table 1. In general, the formation of the local magnetization is driven by mainly two mechanisms: (i) intra-site exchange interaction,

Table 1. Magnetic moments of the investigated $c(2 \times 2)$ MnX systems as calculated by LMTO-ASA for the Mn and the X atoms in and the X atoms below the surface (X = Cu, Fe, Co, and Ni).

Structure	Mn atom (μ_B)	X atom (μ_B)	1. X layer (μ_B)
FM $c(2 \times 2)$ Mn/Cu(001)	3.83	0.095	<0.01
ferriM $c(2 \times 2)$ Mn/Fe(001)	−2.22	1.01	1.31
FM $c(2 \times 2)$ Mn/Co(001)	2.35	1.31	1.58
ferriM $c(2 \times 2)$ Mn/Co(001)	−2.69	1.02	1.67
FM $c(2 \times 2)$ Mn/Ni(001)	2.90	0.19	0.20

on which the first Hund rule is based and which tends to maximize the spin momentum, and (ii) inter-site exchange due to the overlap of the electron orbitals. The latter mechanism can substantially reduce the local moment and even lead to its complete collapse if the overlap is strong enough compared to the intra-site exchange. The effect of the inter-site overlap strongly depends on the local symmetry, lattice parameter and the type of the atoms in the vicinity. The mentioned ferrimagnetic Fe with fcc structure and Cu lattice parameter is a good example, where the magnetic momentum is known to be considerably reduced as compared to that in ordinary ferromagnetic bcc Fe [40].

Hybridization of Mn and Cu is weak for the Mn minority spin states in $c(2 \times 2)$ MnCu/Cu(001); nevertheless, the majority spin band position coincides with the position of the Cu 3d states and hybridization takes place. The 3d bands in Cu are completely filled and moved away from the Fermi energy. If the atomic type of the substrate material is getting closer to Mn, the 3d bands approach each other and hybridization becomes stronger. Fe is the neighbouring element of Mn in the periodic table and hence the hybridization is intense (compare figure 1).

Comparing these LDOSs as well as former theoretical results [14–16] with the experimental data, a smaller band splitting is predicted by the theory than it is observed in the experiment. This discrepancy was previously attributed to final state effects in the experiment [15, 16]. Further reasons are LSDA effects that overestimate the hybridization in systems with narrow bands of 3d of 4f elements that in turn leads to an underestimation of the total band splitting.

4. The $c(2 \times 2)$ Mn/Fe/Cu system

The growth of Mn on Fe/Cu(001) was studied at two different Fe/Cu(001) coverages, one corresponding to 4 ML Fe/Cu(001) forming a (5×1) superstructure, the other one for a 6 ML Fe/Cu(001) stack with a (2×1) LEED pattern. Figure 2 shows the LEED images at a kinetic energy of 71 eV for the case of the 4 ML (5×1) Fe/Cu(001) stack before and after Mn deposition. The LEED pattern obtained for the Fe/Cu(001) stack were not as sharp as reported in former works [27, 41], where films had been grown at substrate temperatures of 100 K and were annealed later at room temperature [42]. Such a procedure was not applied here in order to speed up preparation. Deposition of half a monolayer of Mn yielded a $c(2 \times 2)$ superstructure with LEED spots that were only slightly broader than the ones of the Fe/Cu(001) substrate. Mn deposition onto a 6 ML (2×1) Fe/Cu(001) system, however, did not lead to a very sharp $c(2 \times 2)$ LEED spots and showed additionally less intense $p(2 \times 2)$ spots. There are two possible reasons for the occurrence of a $p(2 \times 2)$ LEED pattern: (i) a different structure, or (ii) an additional antiferromagnetic ordering of the Mn atoms. Antiferromagnetic ordering should lead to a $c(2 \times 2)$ overstructure [43] and superposition on the already existing $c(2 \times 2)$ Mn/Fe/Cu(001) system may produce a $p(2 \times 2)$ LEED pattern. Structural or magnetic analysis could clarify this finding.
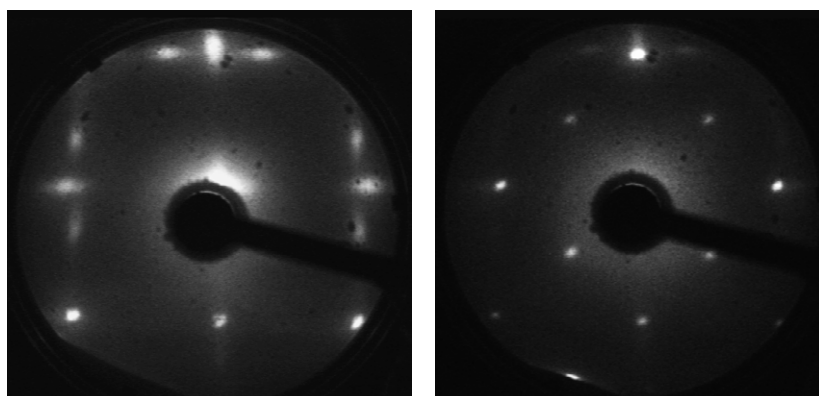
Figure 2. LEED patterns obtained for the 4 ML Fe/Cu(001) system (left-hand side) and 0.5 ML Mn/Fe/Cu(001) (right), respectively, for the kinetic energy of 71 eV.

Our experimental results do not really confirm a c(2 × 2) MnFe surface compound; the formation of such a two-dimensional surface compound, however, is very likely from the existence of such compounds for the Mn/Cu(001) and Mn/Ni(001) systems. Further studies such as LEED I-V investigations or photoelectron diffraction should be used to confirm the compound formation as done in the c(2 × 2) MnCu system [45, 2].

5. Experimental determination of the Mn majority spin band

5.1. Method of determination of the Mn 3d majority spin band position in c(2 × 2) MnCu/Cu(001)

At the centre of the surface Brillouin zone (SBZ), $\bar{\Gamma}$, the position of the Mn 3d majority spin band is expected between 1.55 eV [15] and 3.2 eV [16] BE. Unfortunately, the intense 3d emissions of the underlying Cu substrate appears in the same energy region, masking spectral contributions from the surface compound. Resonant PE has been applied to solve this problem [15]. It is also possible, however, to separate the different spectral contributions by non-resonant PE, taking advantage of the fact that the second c(2 × 2) SBZ reveals an additional $\bar{\Gamma}_{c(2 \times 2)}$ point that does not exist for the p(1 × 1) SBZ (see top inset of figure 3) [17]. Two-dimensional states that are characteristic for the $\bar{\Gamma}$ point of the first c(2 × 2) SBZ should be visible at all possible $\bar{\Gamma}_{c(2 \times 2)}$ points, too. This does not hold, however, for bulk emissions from the Cu substrate emissions. In the following a simple model of a superposition of the Cu(001) substrate and the c(2 × 2) MnCu surface compound emission is applied. Figure 3 shows possible initial state $\vec{k}$-positions in the $\Gamma X W$ plane of Cu(001) calculated for different photon energies and emission angles, treating the final states as free-electron-like[5]. For the measurements at the $\bar{\Gamma}$ point of the first and second c(2 × 2) SBZs, Cu substrate emissions from $\vec{k}$-points along the ΓX and $X W$ directions have to be considered. Results of band structure calculations for Cu along these directions are displayed in the lower inset in figure 3. The best position to separate contributions of the c(2 × 2) surface compound from Cu bulk emissions is obviously near the 3D X-point since there the copper bands reveal a huge energy gap. The X-point is accessible in normal emission with a photon energy of approximately 100 eV in the

---

[5] The assumption of a free electron final state is a rough approximation (see [44]) and is here used only to describe the experimental method.
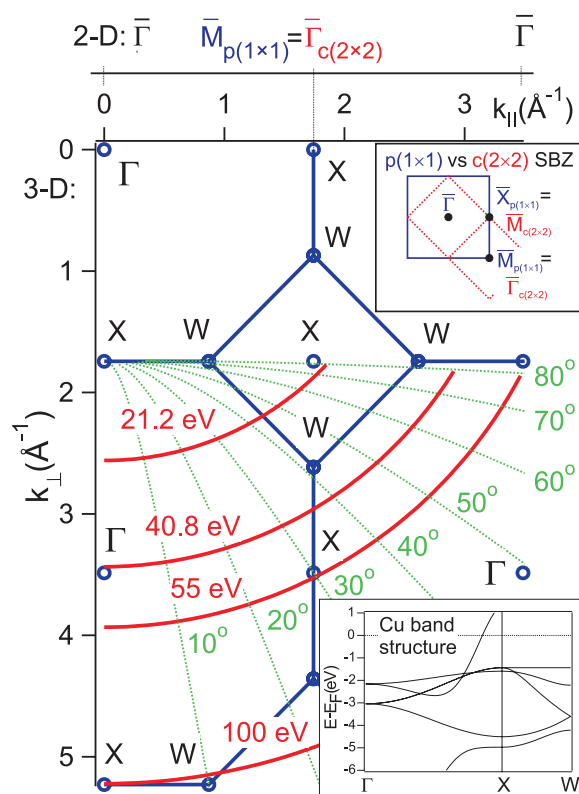
Figure 3. Cut through the ΓXW plane of Cu(001): sphere sectors denote possible free-electron final states for several photon energies. The top inset compares the $p(1 \times 1)$ and the $c(2 \times 2)$ surface Brillouin zones, the latter one revealing an additional $\bar{\Gamma}_{c(2\times2)}$ point of the second SBZ. In the bottom inset theoretical Cu band structure along the $\Gamma-X-W$ directions is shown.

first SBZ and with approximately 20 eV and an emission angle of nearly 80° or 55 eV and 30° in the second SBZ. Advantages of the latter two geometries are better $\vec{k}$ and energy resolutions due to lower photon energies and an enhanced surface sensitivity due to lower photon energies and higher emission angles. Respective experimental results are displayed in figure 4 for $c(2 \times 2)$ MnCu/Cu(001). While almost no differences to pure Cu are visible in PE spectra taken at the $\bar{\Gamma}$-point of the first SBZ ($\theta = 0°$), PE spectra taken with 21.2 eV ($\theta = 66°$) and 55 eV photon energy ($\theta = 30°$) near the centre of the second SBZ reveal a shoulder at 3.0 eV that is attributed to emissions from the Mn 3d majority spin band [17]. At 40.8 eV photon energy and $\theta = 36°$ ($\bar{\Gamma}_{c(2\times2)}$ of the second SBZ) this feature is not resolved in agreement with the above considerations. Here the Cu substrate emissions prevent the determination of the Mn band.

5.2. Mn 3d majority spin band in 0.5 ML $c(2 \times 2)$ Mn/X(001) (X = Fe, Co, Ni)

The same method can be applied to the other $c(2 \times 2)$ MnX (X = Fe, Co, Ni) systems grown on X/Cu(001). PE results from the Mn/4 ML Fe/Cu(001), Mn/6 ML Co/Cu(001), and Mn/6 ML Ni/Cu(001) systems are displayed in figures 5(a), (b), and (c), respectively. The main spectral features between 2 and 4 eV BE in the spectra of Fe/Cu, Co/Cu, and Ni/Cu stem from
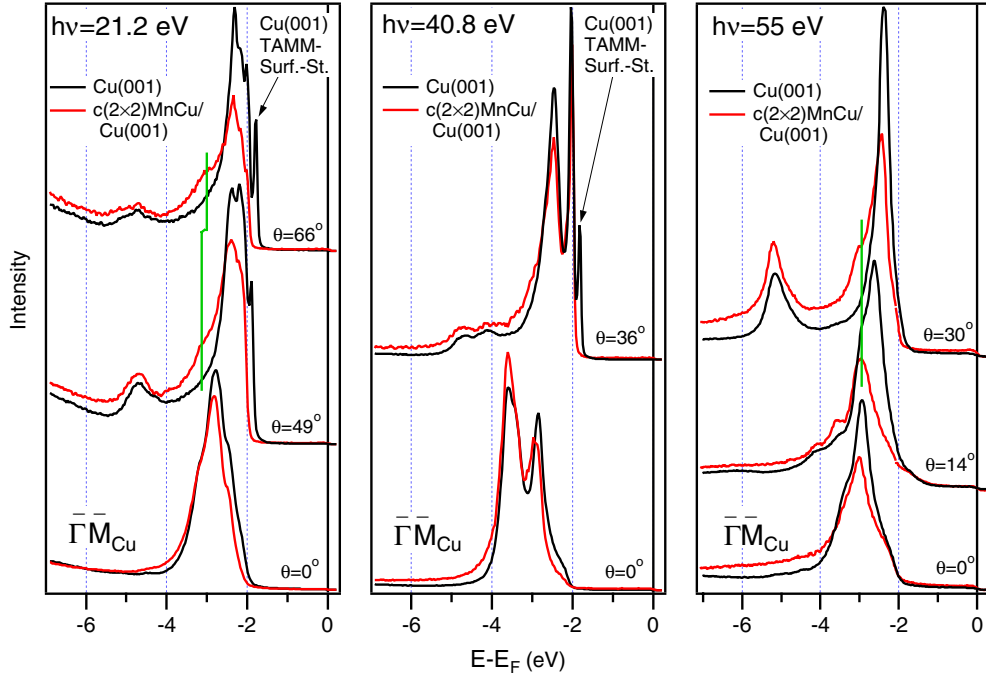
Figure 4. Photoemission spectra of c(2 × 2) MnCu/Cu(001) measured for different photon energies and emission angles. For $h\nu = 21.2$ eV and $\theta = 66°$ as well as for $h\nu = 55$ eV and $\theta = 30°$ one measures close to the X point of Cu(001).

the Cu substrate (compare figure 4). The Cu emission is still visible due to the relatively low kinetic energy ($E_{\text{kin}} \approx 13$ eV).

We want to point out that on the basis of our measurements a possible surface segregation of Cu through the transition metal films cannot be ruled out. Former investigations found only small amounts of Cu segregation to the surface in X/Cu(001) (X = Fe, Co, Ni) of the investigated thickness (see introduction). However, small amounts of copper alone are not able to form a surface compound with a c(2 × 2) LEED pattern of the observed quality since this geometry depends critically on surface stoichiometry [3]. Thus, a formation of the c(2 × 2) overstructure due to a direct interaction of Mn with the magnetic transition metals is concluded. While Mn emissions of MnCu lead only to a shoulder at 3.0 eV, in the PE spectra for c(2 × 2) Mn/Fe/Cu(001) and c(2 × 2) Mn/Co/Cu(001) fully resolved peaks at 3.55 eV BE are observed at $\bar{\Gamma}_{c(2\times2)}$ of the second SBZ. Due to their similarities these peaks are interpreted as Mn 3d majority spin bands. In the Mn/Ni/Cu(001) system emissions at 3.5 eV BE are also attributed to Mn. Rader *et al* observed for a Mn/30 ML Ni/Cu(001) system and normal emission geometry a peak at 3.2 eV BE using 27 eV photon energy [15]. For comparison, we prepared a c(2 × 2) MnNi surface compound on the (001) surface of a Ni single crystal. Figure 5(d) shows spectra near the $\bar{\Gamma}$ point of the first and second SBZs. PE spectra of Ni(001) and c(2 × 2) MnNi/Ni(001) are very similar to each other at normal emission and comparable to the Ni/Cu system, neglecting the Cu substrate emission in Ni/Cu. At the $\bar{\Gamma}_{c(2\times2)}$-point of the second SBZ in c(2 × 2) MnNi/Ni(001), however, two very weak additional peaks appear, one at 3.0 eV and another one at 1.2 eV BE. Both features do not reveal strong dispersion with $k_\parallel$. In analogy to the other c(2 × 2) systems the peak at 3.0 eV is interpreted as part of the Mn 3d majority spin band and, thus, shifted from the position in Mn/Ni/Cu. This peak cannot
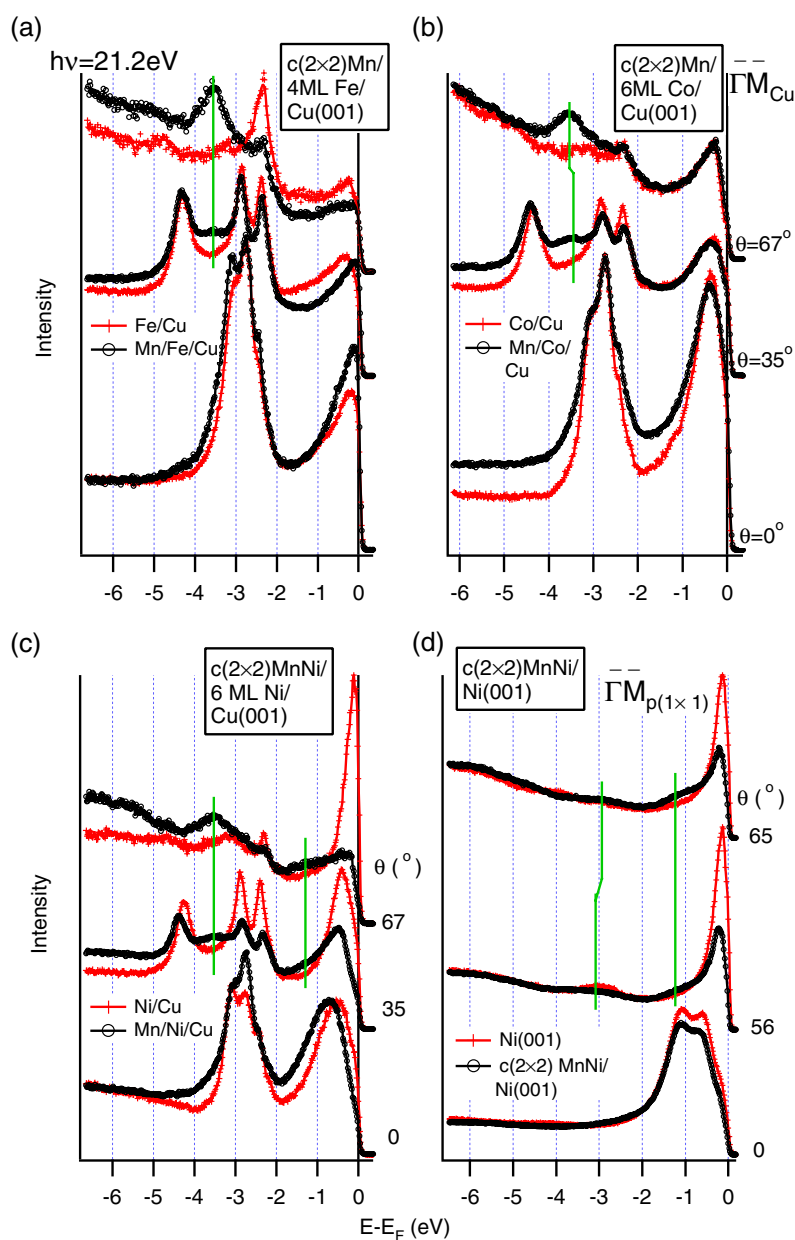
Figure 5. (a)–(c) Photoemission spectra of c(2 × 2) Mn/Fe, c(2 × 2) Mn/Co and c(2 × 2) MnNi/Ni surfaces, respectively, that have been grown epitaxially on Cu(001), and (d) c(2 × 2) MnNi/Ni(001) measured with $h\nu = 21.2$ eV along the $\bar{\Gamma}\bar{M}$ substrate direction.

be observed at normal emission due to the increased bulk-sensitivity of the experiment. The peak at 1.2 eV BE is not only visible for Mn/Ni(001) but also at higher emission angles in the Mn/Ni/Cu system: there, however, only in the form of an intensity enhancement. According to the layered DOS of the Mn/Ni system shown in figure 1 and the calculations of Spišák and Hafner [46] this 1.2 eV feature should be interpreted as an additional branch of the Mn 3d

Table 2. Summary of the Mn 3d majority (↑) and minority (↓) spin band positions for the investigated structures. Values from [15] are marked with an asterisk *.

Structure	$E(\text{Mn } 3d^\uparrow)$ (eV)	$E(\text{Mn } 3d^\downarrow)$ (eV)	ΔE_{tot} (eV)
c(2 × 2) Mn/Fe/Cu(001)	−3.55	—	—
c(2 × 2) Mn/Co/Cu(001)	−3.55	—	—
c(2 × 2) Mn/6 ML Ni/Cu(001)	−3.5	—	—
c(2 × 2) Mn/25 ML Ni/Cu(001)	−3.2*	—	—
c(2 × 2) Mn/Ni(001)	−3.0	2.05*	5.05
c(2 × 2) Mn/Cu(001)	−3.0	1.85*	4.85

majority spin bands. On the other hand minority spin character cannot be ruled out either on the basis of our measurements.

Taking into account the energy position of the unoccupied Mn-derived 3d minority spin band position at 2.05 eV above E_F [15] a total band splitting of 5.05 eV for c(2 × 2) MnNi/Ni(001) can be concluded.

Table 2 summarizes the energy positions at the $\bar{\Gamma}$-point of the occupied majority and unoccupied minority Mn 3d spin bands of the c(2 × 2) systems studied. For the majority spin bands the following may be concluded: (i) the energy positions of these bands are very similar in all three MnX/X/Cu(001) systems (approximately 3.5 eV BE) but different from that one of the Mn/Cu system, but (ii) there exist three different values for the Mn/Ni system depending on the thickness of the substrate. The differences to MnCu may be attributed to hybridization: only copper reveals 3d-derived bands in the energy region around 3 eV, while Fe, Co, and Ni 3d bands are found around the Fermi energy. Therefore, particularly for the Mn/Cu system hybridization effects are important, resulting in a shift of the Mn 3d-derived band to lower BE. Interactions of the Mn majority spin band with the transition metal d-bands located close to the Fermi energy are obviously small, leading to a BE position independent from the choice of the transition element. The thickness dependence (ii) of the energy position of the Mn-derived majority spin band in the Mn/Ni system is most likely due to the variation of the lattice constant. For thin Ni layers the base lattice constant is still the one of the copper substrate (a_{Cu} = 3.61 Å), while thicker films like the ones used by Rader *et al* are expected to relax, leading to a lattice constant between that of Cu and Ni (a_{Ni} = 3.52 Å). A decrease of the interatomic Mn distances increases the Mn 3d overlap and thereby decreases the exchange splitting, an effect that is reflected by a shift of the majority spin band to lower BE.

6. Conclusions

A comparative PE study has been performed on c(2 × 2) surface compounds formed by deposition of 0.5 ML Mn on fcc-(001) surfaces of Fe, Co, Ni, and Cu. Respective transition metal substrates were grown epitaxially as thin films on Cu(001). In all cases LMTO-ASA density of states calculations predict a magnetic split 3d band of Mn for the c(2 × 2) MnX/X(001) surface compound (X = Fe, Co, Ni). For the transition metal compounds the calculated magnetic moments vary between 2.2 and 2.9 μ_B and are lower as for c(2 × 2) MnCu/Cu(001) (3.8 μ_B).

The Mn 3d majority spin band at $\bar{\Gamma}$ is found around 3.5 eV in the three MnX/X/Cu(001) systems (X = Fe, Co, Ni) while the respective states in c(2 × 2) MnCu/Cu(001) and c(2 × 2) MnNi/Ni(001) are observed at 3.0 eV binding energy. The difference is explained in terms of hybridization with the Cu 3d states and the reduced lattice constant of bulk Ni as compared to Ni/Cu(001) thin films, respectively.

Future investigations should include analysis of the magnetic properties in order to verify the obtained results.

Acknowledgment

References

[1] Flores T, Hansen M and Wuttig M 1992 *Surf. Sci.* **279** 251
[2] Toomes R *et al* 1996 *J. Phys.: Condens. Matter* **8** 10231
[3] Wuttig M, Knight C C, Flores T and Gauthier Y 1993 *Surf. Sci.* **292** 189
[4] Wuttig M, Gauthier Y and Blügel S 1993 *Phys. Rev. Lett.* **70** 3619
[5] van der Kraan R G P and van Kempen H 1995 *Surf. Sci.* **338** 19
[6] Banerjee S *et al* 1997 *Surf. Rev. Lett.* **4** 1131
[7] Gallego S *et al* 2003 *J. Phys.: Condens. Matter* **15** 1183
[8] Choi B C, Bode P J and Bland J A C 1998 *Phys. Rev.* B **58** 5166
[9] O'Brien W L and Tonner B P 1995 *Phys. Rev.* B **51** 617
[10] Schmitz D, Rader O, Carbone C and Eberhardt W 1996 *Phys. Rev.* B **54** 15352
[11] Choi B C, Bode P J and Bland J A C 1999 *Phys. Rev.* B **59** 7029
[12] O'Brien W L, Zhang J and Tonner B P 1993 *J. Phys.: Condens. Matter* **5** L515
[13] Huttel Y, Teodorescu C M, Bertran F and Krill G 2001 *Phys. Rev.* B **64** 094405
[14] Fabricius G, Llois A M, Weissmann M, Khan M A and Dreyssé H 1995 *Surf. Sci.* **331–333** 1377
[15] Rader O *et al* 1997 *Phys. Rev.* B **55** 5404
[16] Eder M, Hafner J and Moroni E G 2000 *Phys. Rev.* B **61** 11492
[17] Schiller F, Danzenbächer S and Laubschat C 2001 *Surf. Sci.* **482–485** 442
[18] Wortmann D, Heinze S, Bihlmayer G and Blügel S 2000 *Phys. Rev.* B **62** 2862
[19] Schiller F, Halilov S V and Laubschat C 2003 *Phys. Rev.* B **67** 214431
[20] Binns C and Norris C 1982 *Surf. Sci.* **116** 338
[21] Huttel Y, Schiller F, Avila J and Asensio M C 2000 *Phys. Rev.* B **61** 4948
[22] Schiller F, Halilov S V and Laubschat C 2002 *Phys. Rev.* B **65** 184430
[23] Schneider C M *et al* 1990 *Phys. Rev. Lett.* **64** 1059
[24] Kief M T and Egelhoff W F Jr 1993 *Phys. Rev.* B **47** 10785
[25] Nouverné F *et al* 1999 *Phys. Rev.* B **60** 14382
[26] O'Brien W L and Tonner B P 1994 *J. Appl. Phys.* **76** 6468
[27] Müller S *et al* 1995 *Phys. Rev. Lett.* **74** 765
[28] Wuttig M and Thomassen J 1993 *Surf. Sci.* **282** 237
[29] Huang F, Kief M T, Mankey G J and Willis R F 1994 *Phys. Rev.* B **49** 3962
[30] Shen J, Giergiel J and Kirschner J 1995 *Phys. Rev.* B **52** 8454
[31] Farle M, Platow W, Anisimov A N, Poulopoulos P and Baberschke K 1997 *Phys. Rev.* B **56** 5100
[32] Uiberacker C, Zabloudil J, Weinberger P, Szunyogh L and Sommers C 1999 *Phys. Rev. Lett.* **82** 1289
[33] Mankey G J, Subramanian K, Stockbauer R L and Kurtz R L 1997 *Phys. Rev. Lett.* **78** 1146
[34] Pampuch C, Rader O, Kläsges R and Carbone C 2001 *Phys. Rev.* B **63** 153409
[35] Spišák D and Hafner J 2000 *J. Phys.: Condens. Matter* **12** L139
[36] Kim S H *et al* 1997 *Phys. Rev.* B **55** 7904
[37] Andersen O K 1975 *Phys. Rev.* B **12** 3060
[38] Noguera A, Bouarab S and Dreysse H 1996 *J. Magn. Magn. Mater.* **156** 21
[39] Spišák D and Hafner J 2000 *Phys. Rev.* B **61** 11569
[40] Pinski F J, Staunton J, Gyorffy B L, Johnson D D and Stocks G M 1986 *Phys. Rev. Lett.* **56** 2096
[41] Xhonneux P and Courtens E 1992 *Phys. Rev.* B **46** 556
[42] Steigerwald D A, Jacob I and Egelhoff W F Jr 1988 *Surf. Sci.* **202** 472
[43] Tamura E, Blügel S and Feder R 1988 *Solid State Commun.* **65** 1255
[44] Strocov V N *et al* 2001 *Phys. Rev.* B **63** 205108
[45] Wuttig M, Knight C C, Flores T and Gauthier Y 1993 *Surf. Sci.* **292** 189
[46] Spišák D and Hafner J 1999 *J. Phys.: Condens. Matter* **11** 6359